RESEARCH ARTICLE

Response of sediment microbial community structure in a freshwater reservoir to manipulations in oxygen availability

Lee D. Bryant[1], John C. Little[1] & Helmut Bürgmann[2]

[1]Department of Civil and Environmental Engineering, Virginia Tech, Blacksburg, VA, USA; and [2]Department of Surface Waters – Research and Management, Eawag: Swiss Federal Institute of Aquatic Science and Technology, Kastanienbaum, Switzerland

Correspondence: Helmut Bürgmann, Department of Surface Waters – Research and Management, Eawag: Swiss Federal Institute of Aquatic Science and Technology, CH-6047 Kastanienbaum, Switzerland. Tel.: +41 58 765 2165; fax: +41 58 765 2168; e-mail: Helmut.Buergmann@eawag.ch

Present address: Lee D. Bryant, Department of Surface Waters – Research and Management, Eawag: Swiss Federal Institute of Aquatic Science and Technology, Kastanienbaum, Switzerland.

Received 19 August 2011; revised 11 December 2011; accepted 19 December 2011. Final version published online 20 January 2012.

DOI: 10.1111/j.1574-6941.2011.01290.x

Editor: Riks Laanbroek

Keywords
hypolimnetic oxygenation; lake aeration; sediment–water interface; manganese oxidation; manganese reduction; metal cycling.

Abstract

Hypolimnetic oxygenation systems (HOx) are being increasingly used in freshwater reservoirs to elevate dissolved oxygen levels in the hypolimnion and suppress sediment–water fluxes of soluble metals (e.g. Fe and Mn) which are often microbially mediated. We assessed changes in sediment microbial community structure and corresponding biogeochemical cycling on a reservoir-wide scale as a function of HOx operations. Sediment microbial biomass as quantified by DNA concentration was increased in regions most influenced by the HOx. Following an initial decrease in biomass in the upper sediment while oxygen concentrations were low, biomass typically increased at all depths as the 4-month-long oxygenation season progressed. A distinct shift in microbial community structure was only observed at the end of the season in the upper sediment near the HOx. While this shift was correlated to HOx-enhanced oxygen availability, increased TOC levels and precipitation of Fe- and Mn-oxides, abiotic controls on Fe and Mn cycling, and/or the adaptability of many bacteria to variations in prevailing electron acceptors may explain the delayed response and the comparatively limited changes at other locations. While the sediment microbial community proved remarkably resistant to relatively short-term changes in HOx operations, HOx-induced variation in microbial structure, biomass, and activity was observed after a full season of oxygenation.

Introduction

Significant environmental variability may be observed at the sediment–water interface (SWI) in aquatic systems because of the extremely steep gradients in chemical and physical properties and the related biogeochemical transformation processes that occur in this zone (Santschi *et al.*, 1990). In particular, microbial activity rapidly depletes the dissolved electron acceptors that may be available in the water, for example, dissolved oxygen (O_2) and nitrate (NO_3^-), within just a few millimeters below the SWI. Fe- and Mn-oxides deposited by sedimentation can act as the terminal electron acceptors for organic matter mineralization by specialized microorganisms below the oxic zone (Nealson, 1997; Thamdrup, 2000; Falkowski *et al.*, 2008). Resultant fluxes of reduced chemical species from the sediment, for example, Fe^{2+} and Mn^{2+}, can significantly impair the quality (e.g. color, odor, and taste) of the overlying water and are one of the primary sources of reduced metals in the hypolimnion of stratified lakes and reservoirs (Zaw & Chiswell, 1999; Zhang *et al.*, 1999; Beutel, 2003). It has been shown that microbially mediated sediment–water metal fluxes often have a greater influence on water quality than allochthonous sources (Christian & Lind, 2007).

In light of the imminent water crisis and the acknowledged need for alternative approaches for improving water quality (National Research Council (NRC), 2004),

© 2011 Federation of European Microbiological Societies
Published by Blackwell Publishing Ltd. All rights reserved

FEMS MICROBIOLOGY ECOLOGY

hypolimnetic oxygenation systems (HOx) are being more frequently used to improve water quality by increasing O_2 levels in stratified lakes and reservoirs. While several different types of HOx are used (Singleton & Little, 2006), this work focuses on bubble-plume systems which release air or oxygen gas from diffusers positioned near the reservoir bottom and cause relatively low levels of mixing within the hypolimnion to prevent destratification (Wüest *et al.*, 1992; McGinnis *et al.*, 2004). HOx systems have been shown to not only increase O_2 concentrations and decrease concentrations of soluble metals and other chemical species in the water column (Beutel & Horne, 1999; Gantzer *et al.*, 2009a, b; Liboriussen *et al.*, 2009) but also have significant influence on conditions at the SWI via enhanced sediment O_2 uptake, deepening of the sediment oxic zone, and suppression of soluble metal fluxes within the benthic zone (Beutel, 2003; Bryant *et al.*, 2011a, b). HOx are often used to treat source water with high levels of Mn (Zaw & Chiswell, 1999; Beutel *et al.*, 2007; Gantzer *et al.*, 2009b) which is a serious problem during drinking water treatment because of the complexity of Mn redox kinetics (Kohl & Medlar, 2006; Cerrato *et al.*, 2010). Although the thermodynamic stability of Mn speciation can be predicted, reduced Mn can be persistent in the presence of electron acceptors and often requires a microbial catalyst for oxidation (Balzer, 1982; Dellwig *et al.*, 2012). As a result, Mn speciation in natural waters is known to be strongly dependent on microbial processes (Tebo & Emerson, 1986; Nealson *et al.*, 1988; Lovley, 1991).

Redox kinetics of Fe and Mn are closely paired and often the same organisms carry out both Mn and Fe reduction (Nealson & Saffarini, 1994). It has been suggested that the metal-reducing bacterium *Geobacter metallireducens* and related *Geobacteraceae* may have a dominant role in biogeochemical cycling of Fe and Mn at the SWI in lakes and reservoirs (Thamdrup, 2000; Cummings *et al.*, 2003). Even in well-oxygenated, lacustrine environments, *G. metallireducens*, which are obligate anaerobes, can thrive in the suboxic sediment immediately below the SWI (Coppi *et al.*, 2001). These bacteria acquire energy for anaerobic growth by coupling the oxidation of organic matter with the reduction of Fe^{3+} or Mn^{4+} from various oxides and hydroxides, although other electron acceptors such as NO_3^- may also be used (Thamdrup, 2000).

It is established that sediment microbial communities can change in terms of both population size and structure as a function of sediment O_2 availability (House, 2003). In general, redox conditions and the availability of electron acceptors are natural drivers of microbial community composition and the dominating microbial processes (Nealson, 1997; Koizumi *et al.*, 2004). HOx-induced variation in the extent of the sediment oxic zone (Bryant *et al.*, 2011a) may thus have significant influence on sediment microbial community structure and biologically controlled redox processes. Furthermore, while biogeochemical cycling of metals at the SWI is frequently governed by sediment microbial activity (Santschi *et al.*, 1990; DiChristina & DeLong, 1993; Stein *et al.*, 2001), very little is known about how dynamic changes in environmental conditions (e.g. variations in O_2 availability) affect microbial communities and associated redox processes (Yannarell *et al.*, 2003; Christian & Lind, 2007; Angeler, 2009). It has been shown that the vertical O_2 distribution across the SWI can be significantly influenced by both natural (e.g. wind-driven seiching) and mechanical (e.g. oxygenation) processes (Lorke *et al.*, 2003; Bryant *et al.*, 2010, 2011a). While HOx-induced changes in chemical and physical controls on sediment O_2 uptake and soluble metal fluxes have been evaluated in previous work (Beutel, 2003; Bryant *et al.*, 2011a, b), the influence on sediment microbial populations and processes has not been assessed. We therefore evaluated how sediment microbial community structure responded on a reservoir-wide scale to changes in HOx operation and subsequent Fe, Mn, and O_2 dynamics at the SWI.

Materials and methods

Study site

This work focused on Carvins Cove Reservoir (CCR), one of the primary drinking water supply reservoirs for the

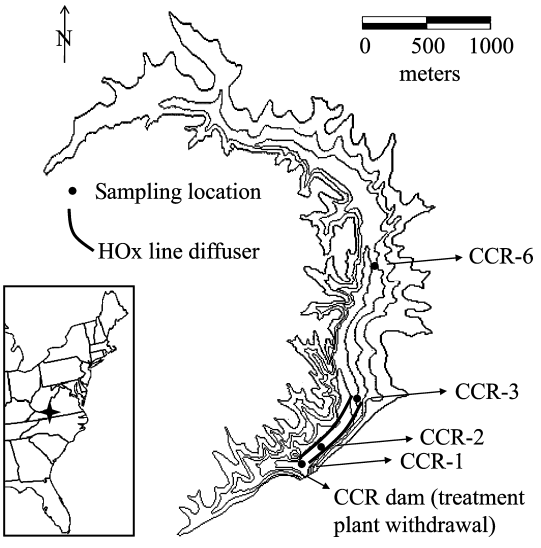

Fig. 1. Map of CCR. The map shows the location of the linear bubble-plume HOx and sampling sites. Near-field locations include CCR-1 (0 m; relative to beginning of HOx lines) and CCR-2 (189 m); central, mid-reservoir locations include CCR-3 (683 m) and CCR-6 (1814 m). Modified from Bryant *et al.* (2011a).

© 2011 Federation of European Microbiological Societies
Published by Blackwell Publishing Ltd. All rights reserved

county of Roanoke, VA, USA. CCR is eutrophic (average total phosphorus ~ 50–70 μg L^{-1}; P.A. Gantzer, pers. commun.) with a maximum depth of ~ 23 m, width of ~ 600 m, and length of ~ 8000 m (Fig. 1). In 2005, a linear bubble-plume diffuser HOx operated with pure oxygen gas was installed by the Western Virginia Water Authority in the deepest section of the reservoir (Fig. 1). Oxygenation was implemented in CCR to replenish O_2 depleted during summer stratification and to decrease Fe and Mn levels in the source water (McGinnis & Little, 2002; Gantzer *et al.*, 2009a). A considerable improvement in source water quality has been observed since HOx operations began, with soluble Mn levels decreasing by > 97% (Gantzer *et al.*, 2009b). Data were collected from 2005 through 2008 to evaluate the influence of the HOx on CCR (Gantzer *et al.*, 2009a, b; Bryant *et al.*, 2011a, b). During the 2006 CCR oxygenation season, on which this study is largely focused, HOx oxygen-gas flow was increased incrementally from 0 to 85 m^3 h^{-1} over a 5-month period (June–October; Fig. 2).

Sediment sampling

Sediment cores were obtained at near-field sites CCR-1 and CCR-2 and upstream at mid-reservoir sites CCR-3 and CCR-6 (sample codes 1, 2, 3, and 6, respectively; Table 1), thereby characterizing the region from directly alongside the HOx to ~ 2000 m upstream of the HOx (Fig. 1). Sampling was performed at four times coinciding with changes in HOx flow rate during the 2006 oxygenation season (12 July, 2 August, 28 August, and 19 October; sample codes A–D; Table 1). Per the HOx flow and sampling regime (Fig. 2), sediment samples were obtained at the end of the month-long anoxic period after the HOx had been turned off and at three points during the subsequent oxic period after oxygenation was resumed. On each sampling date, three undisturbed sediment cores were obtained from each site. One core was used for O_2 microprofile measurements, one for bulk sediment analyses, and one for microbial analyses. A sediment core was also obtained from each site during follow-up work in 2007 to specifically evaluate the presence of Mn-oxidizers in CCR sediment. Sediment cores, obtained using a 90-mm diameter Uwitec corer following Bryant *et al.* (2011b), were considered undisturbed based on clarity of the overlying water (i.e. absence of resuspended sediment) and visual inspection of the sediment surface. Cores were kept in the dark and on ice during transport to the laboratory.

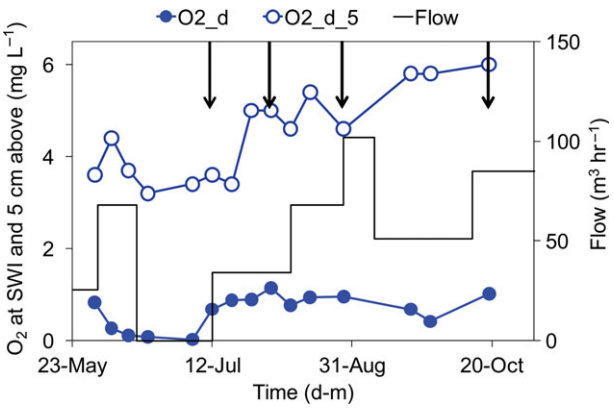

Fig. 2. HOx oxygen-gas flow rates, dissolved oxygen (O_2; parameter O2_d in Table 3) at the SWI, O_2 at 5 cm above the SWI (O2_d_5; Table 3), and dates of sampling. The HOx was turned off from mid-June to mid-July 2006 to establish anoxic conditions. Oxygenation was then resumed and flow was increased incrementally to the maximum possible flow rate (~ 100 m^3 h^{-1}). Sediment cores were collected on dates indicated by vertical black arrows. Average data are shown in figure; corresponding variability in data is presented in Table S1 (Supporting Information).

Core subsamples (~ 12 mL) for microbial analyses were collected within ~ 2 h of sampling at the following depth intervals: 0–2, 2–4, 4–6, and 10–12 mm (sample codes a–d; Table 1) relative to the sediment surface (SWI = 0 mm). Subsamples were immediately placed in sterile glass bottles, sealed, and frozen at −80 °C until analysis (excluding 3 days while being shipped frozen and encased in ice packs to Eawag, where microbial work was performed).

Sediment porewater measurements

O_2 porewater data (O2_d) were obtained via O_2 microsensor profiles of sediment cores following Bryant *et al.* (2011b). Sediment cores were cut to a height of ~ 20 cm for profiling using a Uwitec core-cutter. Care was taken to ensure sediment cores remained undisturbed during the cutting process. Cores were profiled typically within 1–2 h of sampling using Clark-type O_2 microsensors (OX-100; Unisense A/S, Aarhus, Denmark) which have an internal reference and a guard cathode. OX-100 microsensors have an extremely small tip size and depth resolution (100 μm), rapid response time (90% response in < 10 s), and negligible stirring sensitivity. The microsensors were manually controlled by a micromanipulator (M3301R; World Precision Instruments, Inc., Sarasota, FL) and were used in coordination with a high-sensitivity picoammeter (PA2000; Unisense A/S). Mild stirring of the core surface water was maintained during profiling to prevent the water column from becoming stagnant while also minimizing the introduction of artificial turbulence (Glud, 2008). Cores were profiled at 1-mm depth resolution from 5 cm above to 1 cm below the SWI; for each profile, three

© 2011 Federation of European Microbiological Societies
Published by Blackwell Publishing Ltd. All rights reserved

Table 1. Sediment sampling strategy and nomenclature used in microbial analytical techniques

Location	Depth (mm)	Date	RDA-label	Location	Depth (mm)	Date	RDA-label
CCR-1	0–2	7/12/06	1Aa	CCR-3	0–2	7/12/06	3Aa
CCR-1	2–4	7/12/06	1Ab	CCR-3	2–4	7/12/06	3Ab
CCR-1	4–6	7/12/06	1Ac	CCR-3	4–6	7/12/06	3Ac
CCR-1	10–12	7/12/06	1Ad	CCR-3	10–12	7/12/06	3Ad
CCR-1	0–2	8/2/06	1Ba	CCR-3	0–2	8/2/06	3Ba
CCR-1	2–4	8/2/06	1Bb	CCR-3	2–4	8/2/06	3Bb
CCR-1	4–6	8/2/06	1Bc	CCR-3	4–6	8/2/06	3Bc
CCR-1	10–12	8/2/06	1Bd	CCR-3	10–12	8/2/06	3Bd
CCR-1	0–2	8/28/06	1Ca	CCR-3	0–2	8/28/06	3Ca
CCR-1	2–4	8/28/06	1Cb	CCR-3	2–4	8/28/06	3Cb
CCR-1	4–6	8/28/06	1Cc	CCR-3	4–6	8/28/06	3Cc
CCR-1	10–12	8/28/06	1Cd	CCR-3	10–12	8/28/06	3Cd
CCR-1	0–2	10/19/06	1Da	CCR-3	0–2	10/19/06	3Da
CCR-1	2–4	10/19/06	1Db	CCR-3	2–4	10/19/06	3Db
CCR-1	4–6	10/19/06	1Dc	CCR-3	4–6	10/19/06	3Dc
CCR-1	10–12	10/19/06	1Dd	CCR-3	10–12	10/19/06	3Dd
CCR-2	0–2	7/12/06	2Aa	CCR-6	0–2	7/12/06	6Aa
CCR-2	2–4	7/12/06	2Ab	CCR-6	2–4	7/12/06	6Ab
CCR-2	4–6	7/12/06	2Ac	CCR-6	4–6	7/12/06	6Ac
CCR-2	10–12	7/12/06	2Ad	CCR-6	10–12	7/12/06	6Ad
CCR-2	0–2	8/2/06	2Ba	CCR-6	0–2	8/2/06	6Ba
CCR-2	2–4	8/2/06	2Bb	CCR-6	2–4	8/2/06	6Bb
CCR-2	4–6	8/2/06	2Bc	CCR-6	4–6	8/2/06	6Bc
CCR-2	10–12	8/2/06	2Bd	CCR-6	10–12	8/2/06	6Bd
CCR-2	0–2	8/28/06	2Ca	CCR-6	0–2	8/28/06	6Ca
CCR-2	2–4	8/28/06	2Cb	CCR-6	2–4	8/28/06	6Cb
CCR-2	4–6	8/28/06	2Cc	CCR-6	4–6	8/28/06	6Cc
CCR-2	10–12	8/28/06	2Cd	CCR-6	10–12	8/28/06	6Cd
CCR-2	0–2	10/19/06	2Da	CCR-6	0–2	10/19/06	6Da
CCR-2	2–4	10/19/06	2Db	CCR-6	2–4	10/19/06	6Db
CCR-2	4–6	10/19/06	2Dc	CCR-6	4–6	10/19/06	6Dc
CCR-2	10–12	10/19/06	2Dd	CCR-6	10–12	10/19/06	6Dd

Sample identifiers are based on the first digit to identify location (1, 2, 3, and 6 identifying sites CCR-1, CCR-2, CCR-3, and CCR-6, respectively), followed by an uppercase letter identifying sampling date in chronological order (i.e. 'A' represents first sampling date 12 July 2006) and a lowercase letter indicating depth below the sediment surface in order of increasing depth (i.e. 'b' represents second depth from sediment–water interface at 2–4 mm).

measurements were obtained at each depth. Because of the time involved with core processing, single O_2 profiles were obtained per core. Additional single-point measurements of the SWI were also obtained in triplicate after profiling. While this approach may not characterize potential spatial heterogeneity in the sediment O_2 distribution (Glud *et al.*, 2009), sediment core O_2 data were analogous to data obtained under similar conditions with an *in situ* microprofiler during subsequent campaigns in CCR (Bryant *et al.*, 2011a, b). O_2 microsensor data were calibrated using a linear calibration based on O_2 concentrations in the overlying core water (as determined by Winkler titration; Dalsgaard *et al.*, 2000) and in the anoxic sediment.

Soluble Fe and Mn concentrations in the sediment (Fe_s and Mn_s, respectively) were obtained via *in situ* porewater analyzers ("peepers") constructed following Hesslein (1976), Lewandowski *et al.* (2002), and Bryant *et al.* (2011b). Peepers were fabricated using 0.45-μm Millipore (Billerica, MA) filter paper and therefore measured both colloidal (< 0.45 μm) and dissolved (< 0.2 μm) components of soluble (< 0.45 μm) Fe and Mn. Peepers were deployed in duplicate for 2–4 weeks at a time to allow the peepers to come to equilibrium with *in situ* concentrations. Peeper data were obtained only at location CCR-1 because of the limited availability of equipment. Immediately upon retrieval, water samples were obtained via sterilized pipettes from each peeper chamber, transferred to acidified plastic tubes, and analyzed for metals via inductively coupled plasma (ICP) spectroscopy (Clesceri *et al.*, 1998) and for ferrous Fe^{2+} (Fe_f) using the ferrozine method (Stookey, 1970; Viollier *et al.*, 2000).

© 2011 Federation of European Microbiological Societies
Published by Blackwell Publishing Ltd. All rights reserved

Water sample measurements

Because peeper data were measured at site CCR-1 only, near-sediment water samples were used to obtain metals data for all sites. Following protocol by Dalsgaard *et al.* (2000), water samples were taken using a syringe with attached tubing to withdraw water at ~ 5 cm above the sediment from each core designated for bulk sediment sampling. Per sample site and date, individual water samples were obtained for analysis of total metals, soluble metals, and O_2 concentrations. Care was taken not to introduce headspace into the syringe during sampling. All water samples for metal analyses were transferred immediately to plastic bottles and acidified. Near-sediment water samples for soluble Fe and Mn (Fe_s_5 and Mn_s_5, respectively) analyses were first filtered through 0.45-μm Millipore filter paper, while samples for total Fe and Mn (Fe_tot_5 and Mn_tot_5, respectively) analyses were transferred directly (Van Cappellen *et al.*, 1998). After acidifying, samples were then analyzed via ICP (Clesceri *et al.*, 1998). Water samples were analyzed for O_2 concentration at ~ 5 cm above the sediment (O2_d_5) via Winkler titration.

Bulk sediment analyses

The upper ~ 2 cm of sediment of each core designated for bulk sediment sampling was transferred directly into sterile glass containers immediately after obtaining the cores and taking near-sediment water samples. Samples were analyzed following standard methods for total solids (per method SM2540B; Greenberg *et al.*, 1992), total Fe, Mn, and P (Fe_Tot, Mn_Tot, and P_Tot, respectively; per methods SW6010B and SW3050B; Environmental Protection Agency (EPA), 1996), and total organic carbon (TOC; per Lloyd Kahn method; EPA, 1988).

Microbial methods

Nucleic acid extraction from CCR sediment

Nucleic acids were extracted from sediment samples using a slightly modified bead-beating method of Bürgmann *et al.* (2001). 0.5 ± 0.05 g of each sediment sample (Table 1) was used for extraction. For each sample (one per depth from each core designated for microbial analysis), after bead-beating and centrifuging sediment in 1.25 mL CTAB buffer (Bürgmann *et al.*, 2001) at 16 100 ***g*** for 3 min, 400 μL phenol (pH 8) and 400 μL chloroform-isoamyl alcohol (24 : 1; CIA) were added to 1000 μL of sediment extract. After vortexing (15 s) and centrifugation (5 min at 16 100 ***g***), 800 μL of supernatant was combined with 400 μL CIA, re-vortexed (20 s), and centrifuged for 5 min at 16 100 ***g*** 900 μL of supernatant was removed, combined with 900 μL of polyethylene-glycol precipitation solution (Bürgmann *et al.*, 2001), and vortexed briefly. The sample was incubated for 1 h at 37 °C, centrifuged for 30 min at 20 800 ***g***, and the supernatant was removed. The resultant pellet was washed with cold 70% ethanol, centrifuged for 5 min at 16 100 ***g***, and supernatant was again removed (Bürgmann *et al.*, 2001). Nucleic acid extracts were dissolved in 50 μL Tris–EDTA buffer and stored at −20 °C prior to subsequent PicoGreen quantification, PCR amplification, and ribosomal intergenic spacer analysis (RISA).

DNA quantification with PicoGreen

Extracted nucleic acid concentrations were quantified with PicoGreen (Bürgmann *et al.*, 2001) based on the Quant-it dsDNA quantitation kit (Invitrogen, Basel, Switzerland) using a Synergy HT microplate reader (Bio-Tek Instruments, Inc., Winooski, VT). The purity of extracted DNA was assessed spectrophotometrically from the absorbance ratio at 260 and 280 nm. Nucleic acid samples were diluted to concentrations of 5, 10, and 20 ng μL^{-1} for PCR and RISA analyses.

Nucleic acid amplification via PCR

Diluted samples of sediment-extracted nucleic acids were used for all PCR analyses. The general bacterial primer set ARISA-16S-1406f/ARISA-23r (Table 2) was used for PCR amplification of the ribosomal intergenic spacer region for RISA (Borneman & Triplett, 1997; Fisher & Triplett, 1999; Sigler *et al.*, 2002). Additional PCR products were obtained using primers specific to the 16S rRNA genes of *Geobacteraceae* (494f/825r; Table 2), following Holmes *et al.* (2002). Each PCR reaction using ARISA or *Geobacteracea*-specific primers contained 1 μL of sample, 1× PCR buffer, 3 mM $MgCl_2$, 0.2 μM of each primer, 0.2 mM dNTP, 1 mg mL^{-1} bovine serum albumin, 0.25 μL of Taq polymerase, and 32.15 μL of nuclease-free water with a final reaction volume of 50 μL. Following initial denaturation at 94 °C for 5 min, 35 PCR cycles were performed under the following conditions: denaturing at 94 °C for 30 s, annealing at 55 °C for 1 min, extension at 72 °C for 1.5 min, and a 5-min final extension at 72 °C. Amplification products were then visualized on ethidium bromide-stained agarose gel using the GelDoc documentation system (Bio-Rad Laboratories, Reinach, Switzerland) for densitometric screening.

© 2011 Federation of European Microbiological Societies
Published by Blackwell Publishing Ltd. All rights reserved

Table 2. Primers used for nucleic acid amplification via PCR

Primer name	Target	Sequence	Reference
ARISA-16S-1406f	Universal; 16s rRNA gene	5′-TGY ACA CAC CGC CCG T-3′	Yannarell *et al.* (2003)
ARISA-23Sr	Bacteria; 23s rRNA gene	5′-GGG TTB CCC CAT TCR G-3′	Yannarell *et al.* (2003)
494f	*Geobacteraceae*;16s rRNA gene	5′-AGG AAG CAC CGG CTA ACT CC-3′	Holmes *et al.* (2002)
825r	*Geobacteraceae*;16s rRNA gene	5′-TAC CCG CRA CAC CTA GT-3′	Anderson *et al.* (1998)

Sequencing and sequence analysis of *Geobacter* amplicons

Geobacteraceae-specific PCR products of the top sediment layer (0–2 mm below the SWI) of each site for the two end-point sampling dates (7 July and 19 October 2006) were cloned using the pGEM T-easy Vector Systems cloning kit (Promega, Madison, WI) according to manufacturer instructions. All clones were subjected to standard blue-white screening. Five random clones from each library were selected for plasmid extraction using the GenElute HP Plasmid Miniprep Kit (Sigma-Aldrich, St. Louis, MO) and sequenced (Mircorsynth, Balgach, Switzerland).

Sequences were checked for chimera formation using the Bellerophon 3 web service (http://greengenes.lbl.gov/cgi-bin/nph-bel3_interface.cgi). Sequences were uploaded and taxonomically classified using the Classifier tool on the Ribosomal Database Project (RDP) website. Fourteen sequences classified as belonging to *Geobacteraceae* were uploaded and aligned to the RDP database, and closely related type strains were identified using RDP's Seqmatch tool and hierarchy browser. The alignment was downloaded from RDP, and a phylogenetic inference tree was calculated in MEGA 5 (Tamura *et al.*, 2011) using the unweighted pair group method with arithmetic mean (UPGMA) clustering algorithm, Kimura 2-parameter distance metric, and complete elimination of gaps. The resulting tree is based on 335 sites and was tested using 1000 bootstrap resamplings. The 14 *Geobacteraceae* sequences were deposited at GenBank under accession numbers JN098406 through JN098419.

Geobacter real-time PCR

A real-time detection PCR (RTD-PCR) protocol for *Geobacteraceae* targets was performed using *Geobacter*-specific primers 494f and 825r and following Holmes *et al.* (2002; Table 2). Each RTD-PCR reaction contained, in a final volume of 30, 5 μL of sample, 1× SYBR green PCR buffer (Applied Biosystems, Carslbad, CA), 1.2 μM of each primer, 3 mM $MgCl_2$, and 8.1 μL of nuclease-free H_2O. RTD-PCR amplification was performed using an Applied Biosystems 7500 Fast Real-Time PCR System with one cycle at 50 °C for 2 min, one cycle at 95 °C for 10 min, and 45 cycles at 95 °C for 15 s and 56 °C for 1 min, followed by melting-curve analysis. RTD-PCR amplification of genomic DNA extracts of *G. metallireducens* strain GS15 (DSM7210) with primers 494f and 825r was used to create a standard curve (Holmes *et al.*, 2002) based on known concentrations ranging from 6×10^{-7} to 6×10^{3} ng μL^{-1}. The calibration was linear over six orders of magnitude but results from sample dilutions indicated that DNA extracts inhibited the PCR and that PCR inhibition varied between samples. Results therefore were not evaluated quantitatively but scored qualitatively. Each sample was amplified in three different dilutions (5, 10, and 20 ng μL^{-1} DNA). Any sample with positive amplification (fluorescence threshold exceeded) and a correct melting temperature within ±1 °C of the standards (83 °C) was scored as *Geobacteraceae*-positive.

RISA community fingerprints

Banding patterns obtained via RISA were used to characterize the bacterial community structure (Fisher & Triplett, 1999; Sigler *et al.*, 2002). Each band's relative intensity was used as an estimator of relative abundance of each observed phylotype. While the individual abundance of a phylotype may not accurately reflect the abundance of the corresponding bacteria in the original population, for example, because of PCR bias, changes in community composition between samples are generally reliably reflected using this approach (Hartmann *et al.*, 2005; Nocker *et al.*, 2007). 5 μL of RISA amplicons (mixed with 3 μL of bromphenol blue/sucrose loading dye) was loaded onto 5% bis-acrylamide gels. Gel electrophoresis was performed in a 1×TAE buffer at 35 °C for 15 min at 30 V and then 4 h at 200 V. Following electrophoresis, staining was performed by gently agitating the gel in 50 mL of 1×TAE with a 1 : 5000 dilution of SYBR Green dye (Molecular Probes, Inc, Life Technologies, Grand Island, NY) for 30 min. RISA band patterns were then analyzed using the Gel Doc high-resolution gel documentation system and Quantity One software (Bio-Rad Laboratories). Densitometric data for each gel were manually assembled in Microsoft Excel into a single dataset by matching bands between gels based on calculated fragment size. Community analysis results were based either on relative band intensity or on a converted dataset with presence–absence data.

© 2011 Federation of European Microbiological Societies
Published by Blackwell Publishing Ltd. All rights reserved

Statistical analysis

All statistical analyses were performed using the statistical software R (R Development Core Team, 2009) with packages VEGAN (Oksanen *et al.*, 2009) and BIODIVERSITY R (Kindt & Coe, 2005). The influence of site, sediment depth, and time on nucleic acid concentration was analyzed by one- or multi-factorial analysis of variance (ANOVA). Similarity of community structure was assessed via hierarchical cluster analysis (single linkage) using the Bray dissimilarity metric. Additionally, RISA results, which identified patterns of community similarity, were correlated by constrained ordination (Redundancy Analysis; RDA) to several other datasets from the 2006 campaign used as independent environmental variables to explain observed variance in the community fingerprints. Parameters used to define environmental variables are presented in Table 3. Two subsets of data were chosen. The first set included ARISA data from all samples and was analyzed using depth as a covariable in a partial RDA focusing on site- and date-related trends. Constraining variables available for this set were site-specific chemical data for the overlying water, bulk sediment, and depth-resolved O_2 concentrations in the sediment porewater. The second set contained all samples of site CCR-1 (sample ID '1'; Table 1) with depth-resolved peeper and O_2 profile data used as constraining variables. Selection of parsimonious, non-auto-correlated sets of constraints for the statistical models was assisted by forward selection of constraints using VEGAN's ordistep function. Models were tested by permutation analysis (1000 iterations). Passive fitting of variables not included in the RDA model was performed using VEGAN's envfit function. The predictive value of the parsimonious sets of environmental variables was further tested using the Mantel test (Mantel, 1967). For the Mantel test, the matrix of environmental variables was scaled and centered. The Bray dissimilarity was used for the calculation of the distance matrix of the community dataset, and Euclidean distance was used for the environmental dataset. Additionally, the simple Mantel '*r*' was estimated for individual environmental variables.

Table 3. Parameters and corresponding units of environmental variables used in statistical analyses

Environmental variable	Parameter	Units
Sampling site	Distance	m
Sample depth below sediment surface	Depth	mm
Date sample was obtained	Time	–
HOx oxygen-gas flow rate	Flow	$m^3\ h^{-1}$
Soluble Fe obtained via peeper; depth specific on cm scale	Fe_s	mg L^{-1}
Ferrous Fe (Fe^{2+}) obtained via peeper; depth specific on cm scale	Fe_f	mg L^{-1}
Soluble Mn obtained via peeper; depth specific on cm scale	Mn_s	mg L^{-1}
Total Fe in water sample obtained at 5 cm above the sediment	Fe_tot_5	mg L^{-1}
Total Mn in water sample obtained at 5 cm above the sediment	Mn_tot_5	mg L^{-1}
Soluble Fe in water sample obtained at 5 cm above the sediment	Fe_s_5	mg L^{-1}
Soluble Mn in water sample obtained at 5 cm above the sediment	Mn_s_5	mg L^{-1}
Dissolved O_2 in water sample obtained at 5 cm above the sediment	O2_d_5	mg L^{-1}
Dissolved O_2 in porewater; depth specific on mm scale	O2_d	mg L^{-1}
Total Fe in bulk sediment	Fe_tot	mg kg^{-1}
Total Mn in bulk sediment	Mn_tot	mg kg^{-1}
Total P in bulk sediment	P_tot	mg kg^{-1}
TOC in bulk sediment	TOC	mg kg^{-1}

Isolation of Mn-oxidizing bacteria

In 2007, the presence of Mn-oxidizers in CCR sediment was studied based on the leukoberberlin blue (LBB) method following Tebo *et al.* (2007) and Cerrato *et al.* (2010). LBB is a color indicator that chemically reacts with oxidized Mn. Microorganisms were recovered by suspending 1 g of aseptically handled sediment (samples obtained from the upper 2 cm of cores from CCR-1, CCR-2, CCR-3, and CCR-6) in 5 mL sterile tap water contained in a sterile 16 × 125 mm screw-cap tube. A dilution series of recovered samples was prepared in 5 mL sterile tap water (10^{-5} to 10^{-1}), and 0.1 mL from each dilution tube was spread on Mn-oxidation agar plates. The agar media contained 1 mg L^{-1} $FeSO_4 \cdot 7H_2O$, 0.2 g L^{-1} $MnSO_4 \cdot 4H_2O$, 2 g L^{-1} Peptone (Becton Dickinson, Sparks, MD), 0.5 g L^{-1} yeast extract (Becton Dickinson), 10 mM HEPES buffer (pH 7.4), and 15 g L^{-1} Bactoagar, as described by Stein *et al.* (2001). Probable Mn-oxidizers, visually identified as dark-brown or orange irregularly shaped colonies, were selected and streaked to obtain isolates. Fourteen selected isolates were then inoculated in Mn-oxidation broth and incubated at 30 °C. A negative control consisting of sterile Mn-oxidation agar media was maintained to ensure that oxidation observed was biological rather than chemical. Samples were removed weekly, and Mn-oxidation was measured after addition of LBB at a 1 : 5 ratio (Stein *et al.*, 2001). Absorption measurements of isolate samples and controls were obtained using a Hitachi Digital Spectrophotometer (Hitachi High-Technologies America, Inc., Schaumburg, IL) at 620 nm. The calibration curve was prepared from potassium permanganate and LBB.

© 2011 Federation of European Microbiological Societies
Published by Blackwell Publishing Ltd. All rights reserved

Results and discussion

Sediment and water geochemistry

Concentrations of O_2, Fe, and Mn in the sediment and overlying water changed considerably in response to HOx operations. Although a response was observed at all sampling sites, the effect was typically stronger at the near-field sites CCR-1 and CCR-2 because of proximity to the HOx and sediment focusing in the deeper region (Schaller & Wehrli, 1997). Data for all CCR sites are presented in Table S3 (Supporting Information). Results for site CCR-1 are highlighted in Fig. 3. As the oxygenation season progressed and HOx flow rate increased (Fig. 2), O_2 concentrations in porewater and in the water at 5 cm above the sediment were observed to increase throughout CCR (Fig. 3; Table S3). While porewater O_2 data may have been influenced by redox changes occurring during transport and profiling of the cores under *ex situ* conditions, O_2 data obtained via sediment core profiling are comparable to *in situ* data obtained during a subsequent CCR campaign (Bryant *et al.*, 2011a, b), as mentioned previously. Sediment core profiling was advantageous for the current study in that it allowed for clear identification of the SWI and direct correlation of O_2 profile data to core samples used for microbial analyses.

Concentrations of soluble Fe typically decreased in the water at 5 cm above the sediment; trends in soluble Mn concentrations were more variable but concentrations generally increased as the oxygenation season progressed (Bryant *et al.*, 2011b). Similarly, near-field peeper data show that by the end of the oxygenation season porewater concentrations of soluble Fe had decreased by 50% in the upper sediment while concentrations of soluble Mn had increased on average by 130% (Fig. 3; Table S3). Soluble (< 0.45 μm) metal measurements from peepers could have included colloidal (< 0.45 μm) as well as reduced, dissolved (< 0.2 μm) forms of Fe and Mn. Ferrozine results show that the percentage of soluble Fe in the form of reduced Fe_f decreased from 60% to 0% in the upper sediment by the end of the oxygenation season (Table S3). Voltammetric-electrode profiles of sediment cores, obtained during a companion study and following Brendel & Luther (1995), also indicated negligible levels of Fe^{2+} in CCR porewater following continuous oxygenation (LD Bryant, unpublished data); conversely, a majority of porewater Mn remained in the reduced Mn^{2+} form (Bryant *et al.*, 2011b). The differing responses and variation in colloidal fractions of Fe and Mn are likely due to the higher redox potential of Mn^{4+} relative to Fe^{3+} which facilitates Mn to be more easily reduced than Fe in low O_2 environments (Davison, 1985; Nealson & Saffarini, 1994; Jørgensen & Boudreau, 2001). Increased near-sediment and porewater concentrations of Mn may be attributed to the reduction of newly deposited Mn-oxides resulting from HOx-induced sediment loading and subsequent accumulation of particulate matter, confirmed by sediment trap (Gantzer *et al.*, 2009b) and bulk sediment data (Fig. 3; Tables S2 and S3). Trends in bulk sediment data indicate a general increase in levels of total Fe, Mn, and TOC in the near-field sediment over the course of the oxygenation season. Furthermore, bulk sediment levels of total Fe, Mn, and TOC have increased considerably in this region since the start of CCR oxygenation in 2005 (Bryant *et al.*, 2011b; unpublished TOC data).

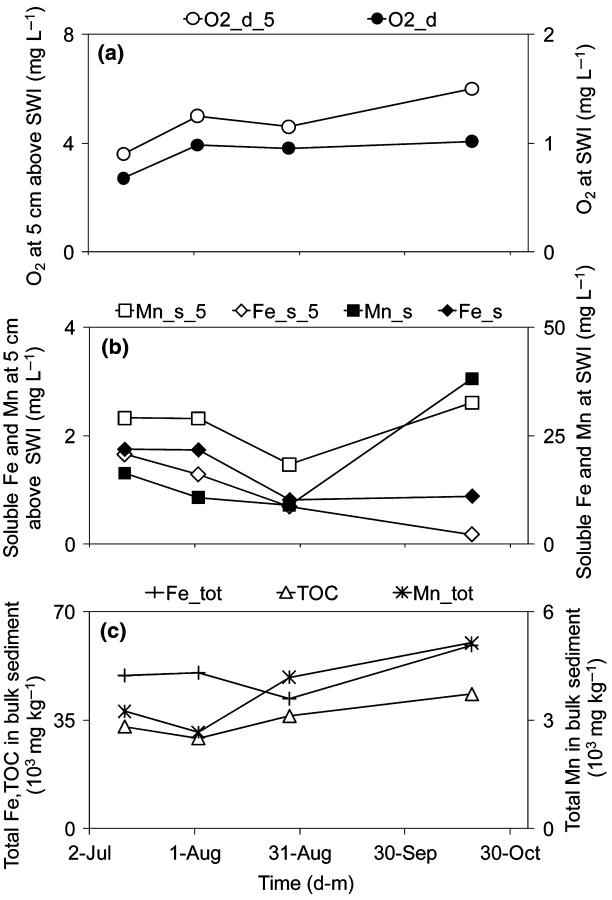

Fig. 3. Temporal variation in chemical parameters at near-field site CCR-1 during the 2006 campaign. (a, b) Variation in O_2 and soluble Fe and Mn at the SWI (O2_d, Fe_s, and Mn_s, respectively) and in the overlying water at 5 cm above the sediment (O2_d_5, Fe_s_5, and Mn_s_5, respectively). (c) Variation in total Fe, Mn, and organic carbon in the bulk sediment (Fe_tot, Mn_tot, and TOC, respectively). All parameter acronyms are defined in Table 3. Average data are shown in figure; corresponding variability in data is presented in Table S2.

© 2011 Federation of European Microbiological Societies
Published by Blackwell Publishing Ltd. All rights reserved

Nucleic acid content of sediment

Previous work has established the use of nucleic acid concentration as an indicator for microbial biomass (Widmer *et al.*, 2006). Although ANOVA did not indicate that sampling site (averaging over depth and time) was a significant ($P < 0.05$) influence by itself, sampling site was found to be significant if time was considered as an additional factor in multivariate ANOVA. Nucleic acid concentration was typically highest at near-field sites CCR-1 and CCR-2 and at CCR-6, the site influenced most directly by HOx plume detrainment in the far field (Fig. 4; Bryant *et al.*, 2011a). Nucleic acid concentrations were consistently lower at CCR-3, the far-field site least affected by the HOx because of distance from the HOx, CCR bathymetry, and plume detrainment. HOx-induced increases in O_2 concentrations at CCR-1, CCR-2, and CCR-6 as well as enhanced levels of TOC and metal oxide precipitation in the near field (discussed below) may thus have supported a denser sediment microbial community in these regions during the campaign.

ANOVA revealed that nucleic acid contents varied significantly ($P < 0.05$) by sampling date across all samples and also in multivariate analyses with either depth or site as additional factors. The date × depth interaction term was also significant indicating that the depth profile varied with sampling date. A sharp decrease in nucleic acid concentrations in the upper sediment layer was observed after the first month of oxygenation during which sediment O_2 levels remained depleted (Fig. 4; Table S3). This may possibly be due to less than optimal growth conditions being maintained for certain groups within the microbial community during this anoxic period (Dellwig *et al.*, 2012). After this initial decrease, nucleic acid concentrations in the surficial sediment typically increased as oxygenation was resumed. Nucleic acid concentrations in the deeper sediment, which were considerably higher than in the upper sediment, also increased at most sites by the end of the campaign (Fig. 4). Correspondingly, trends in O_2 concentrations in the upper sediment indicate increased porewater O_2 throughout the oxygenation season at all locations (Table S3). As the upper sediment became more oxic during oxygenation (Bryant *et al.*, 2011a), enhanced sediment O_2 availability may have increasingly supported microbial growth. Sediment trap data collected at 2 m above the sediment at CCR-1, CCR-2, and CCR-3 confirm that sedimentation rates of total solids, total Fe and Mn, and TOC generally increased throughout the reservoir as the 2006 oxygenation season progressed, particularly in the near field (Gantzer *et al.*, 2009b; Bryant *et al.*, 2011b). This likely resulted from HOx-induced increases in oxidation and subsequent precipitation of Fe- and Mn-oxides and/or enhanced accumulation of organic matter originating from primary production following late-summer phytoplankton blooms. In particular, increased levels of TOC in conjunction with elevated sediment O_2 availability may have enhanced microbial growth. Decreased nucleic acid concentrations in the surficial sediment relative to concentrations in the deeper sediment throughout most of

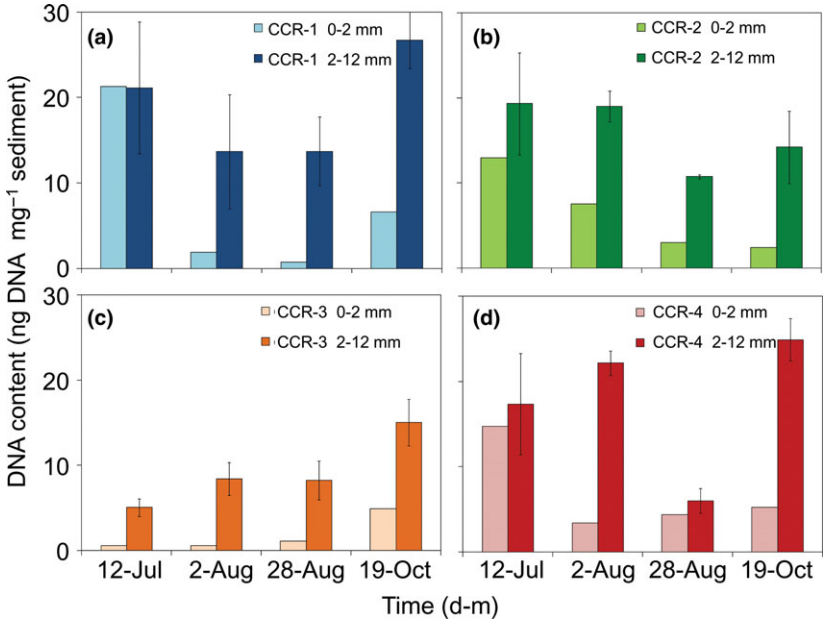

Fig. 4. Nucleic acid concentration data obtained via PicoGreen analyses for sites CCR-1 (a), CCR-2 (b), CCR-3 (c), and CCR-6 (d). Per sampling date, concentration data are presented for the upper sediment where the greatest variation in sediment O_2 concentrations was observed (0–2 mm below the SWI) and for the deeper sediment region (2–12 mm below the SWI). Data shown for the deeper sediment (2–12 mm) are averages based on data from the three sampling depths within this region (Table 1).

© 2011 Federation of European Microbiological Societies
Published by Blackwell Publishing Ltd. All rights reserved

the oxygenation season may be due to the periodic deposition and subsequent accumulation at the sediment surface of material initially rich in Fe- and Mn-oxides and with relatively low microbial biomass.

Microbial community structure

Hierarchical clustering of the RISA community fingerprints shows that a majority of the CCR sediment samples were fairly similar in terms of microbial community structure as indicated by the main cluster highlighted in green in Fig. S1. However, several samples, primarily obtained near the HOx (sites CCR-1 and CCR-2) at the end of the experimental campaign (19 October 2006; sample ID 'D'; Table 1), formed a separate cluster (in orange in Fig. S1). The sediment in the near-field region is influenced by the HOx more directly (Bryant *et al.*, 2011a, b) which could have contributed to the observed shift in community structure. Hypolimnetic O_2 levels remained high throughout the summer (after oxygenation was resumed) and fall prior to fall turnover which occurred in mid-November 2006. An oxic hypolimnion facilitated elevated O_2 in the upper sediment layers and also precipitation of Fe- and Mn-oxide particles as reduced Fe and Mn were oxidized in the water column (Gantzer *et al.*, 2009a, b; Bryant *et al.*, 2011a, b). Enhanced precipitation of organic material may also have occurred. In addition to HOx effects on sediment composition, natural sediment focusing could have been a factor as well. CCR-1 and CCR-2 are located in the deepest part of CCR; thus, this region likely had higher levels of freshly accumulated organic matter and precipitated metal oxides. Bulk sediment data showed that TOC, Fe, and Mn levels were typically higher in the near field than in shallower regions (e.g. CCR-6) farther from the HOx (Bryant *et al.*, 2011b).

The influence of HOx proximity and terrestrial sediment focusing on near-field sediment composition is further supported by the fact that the greatest dissimilarity to the main cluster was observed for samples obtained from the sediment surface from sites CCR-1, CCR-2, and CCR-3 at the end of the oxygenation season (1Da, 2Da, and 3Da; designated in red in Fig. S1). The sediment microbial community in the surficial sediment would obviously have been most directly affected by both accumulation of newly deposited material including fresh, easily degradable organic matter (resulting from HOx operations, algal deposition, and/or sediment focusing) as well as increased hypolimnetic and sediment O_2 levels as oxygenation progressed. These results are in agreement with the nucleic acid content data showing deviation in nucleic acid concentrations in the upper sediment as compared to the deeper sediment (Fig. 4).

Correlation between microbial community structure, geochemical cycling, and HOx operation

RDA (Borcard *et al.*, 2011) based on RISA band intensity data were performed to relate sediment microbial composition to environmental variables (Table 3) and to obtain further insight into trends in community composition. Initially, a partial RDA (with depth as the covariable) based on the full set of RISA data was performed using an environmental dataset based on global experimental and system characteristics available for all sites (Fig. 5). Forward selection of constraining variables indicated Fe_s_5, Mn_tot, and O2_d_5 as a parsimonious set of constraints. The constrained model explained 17% of the unconstrained variance in microbial community structure. The overall model and the contribution of all three constraints were significant according to permutation analysis ($P < 0.01$). Additionally, the Mantel test confirmed a significant influence of the selected variables on the community composition ($r = 0.17$, $P < 0.01$). Individually, O2_d_5 most strongly correlated with the community dataset ($r = 0.18$, $P < 0.05$).

As also indicated by the cluster analysis (Fig. S1), RDA results in Fig. 5 reveal a population shift in the upper sediment samples obtained near the HOx in October (1D, 2D, and 3Da samples; solid ellipsis in Fig. 5) that correlated with the variable O2_d_5. O2_d_5 was directly correlated with HOx flow which is shown as a passively fitted variable in Fig. 5. Moderate correlation between near-field sites and O2_d is also observed. Conversely, a majority of samples from the far-field site CCR-6 appeared somewhat distinct from other samples and far less affected by HOx flow and SWI O_2 levels (dashed ellipsis in Fig. 5). While CCR-6 is directly influenced by the HOx via plume detrainment (Bryant *et al.*, 2011a), it is farther away and is also the shallowest site and therefore less affected by sediment focusing. These RDA results indicate that O_2 levels in the overlying water column, subsequent metal oxide precipitation, and the resulting sediment composition may have been stronger controls on sediment microbial community structure than sediment O_2 availability.

To evaluate the relationship between community composition and porewater geochemical data at different depths, an RDA was performed on a reduced dataset that included only samples from site CCR-1 for which depth-resolved geochemical data (Fe_s, Fe_f, and Mn_s) were available in addition to O_2 profile data (Fig. 6). Forward selection indicated Fe_f and O2_d as parsimonious constraining variables. This RDA explained ~ 29% of the unconstrained variance. The model was significant ($P < 0.05$) with the contribution of Fe_f and O2_d signif-

© 2011 Federation of European Microbiological Societies
Published by Blackwell Publishing Ltd. All rights reserved

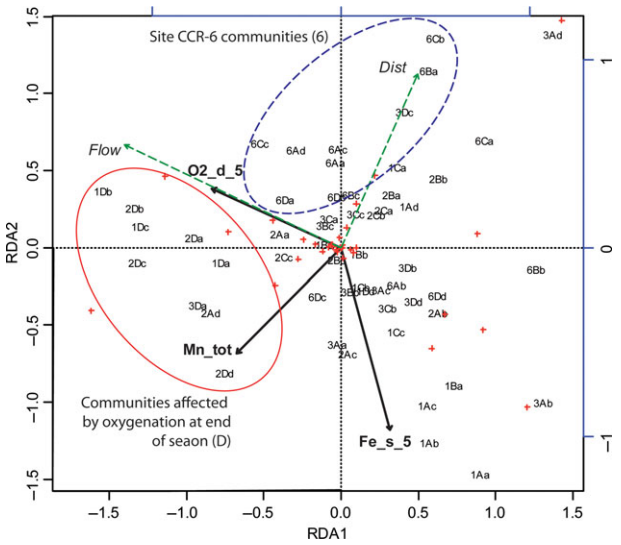

Fig. 5. Triplot of RDA ordination of the RISA community dataset and environmental variables. A partial RDA with a constrained model was used to analyze the full set of CCR samples; depth effects were eliminated by using depth as a covariable. RISA community composition data correlated with the variables near-sediment soluble iron concentration (Fe_s_5), O_2 at 5 cm above the SWI (O2_d_5), and total Mn in the bulk sediment (Mn_tot). Additional variables HOx flow rate (Flow) and distance to HOx (Dist) were passively fitted. Crosses represent individual bacterial phylotypes identified by RISA bands. Samples are coded as listed in Table 1.

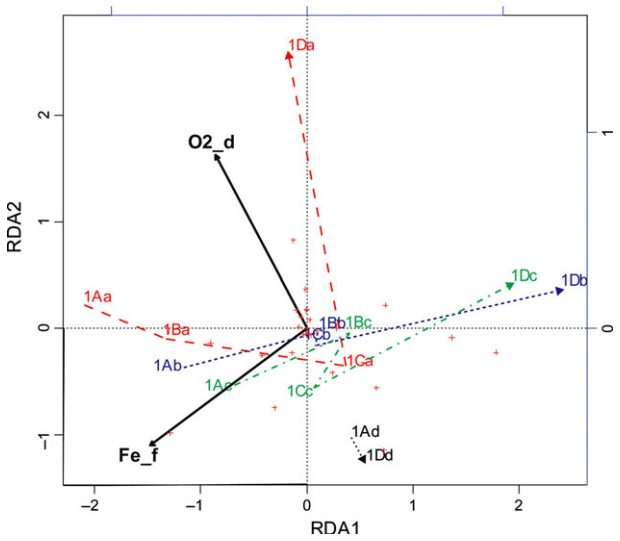

Fig. 6. Triplot of RDA ordination of RISA data from site CCR-1 using depth-resolved geochemical data as constraints. Porewater dissolved oxygen (O2_d) and ferrous iron (Fe_f) correlated with shifts in the microbial community in the upper sediment layers (sample ID XXa–c). The deepest layer (sample ID XXd) remained stable. Dashed arrows show the temporal development of the microbial community at each depth. Samples are coded as listed in Table 1.

icant and marginally significant ($P < 0.1$), respectively. The Mantel test confirmed both a significant correlation of the selected variables with the community dataset ($r = 0.31$, $P < 0.05$) and also the significant and marginally significant influence of the individual variables. This analysis shows the considerable correlation between community structure at site CCR-1 and the biogeochemical conditions. The temporal trend in each sediment layer (as designated by arrows in Fig. 6) shows that the top three sediment layers were highly dynamic over the oxygenation season with the community in the top layer becoming quite dissimilar to the other communities by the end of the oxygenation season. Conversely, the deepest sediment layer remained unaffected (samples 1Ad, 1Dd).

In summary, the multiple RDA explained moderate proportions of the overall variance in the sample set as a function of the environmental and geochemical variables evaluated. The ordination also indicated that community structure was not influenced by an easily discernable trend of one or a few species but rather by independent changes of many phylotypes (Figs 5 and 6). Low percentages of explained variance are not unusual in constrained ordinations of biological data. However, in comparison to results from other ordination studies of environmental microbial communities (Yannarell & Triplett, 2005; Buesing *et al.*, 2009; Bürgmann *et al.*, 2011), a relatively small part of the variance in the community dataset was explained by our RDA ordinations. This may be attributed to the adaptability of the microbial community to transient changes in environmental conditions. Alternatively, microbial community structure may have been influenced by potentially important drivers of microbial community composition that were not considered here (e.g. temperature, pH, food-web properties). During subsequent work in CCR, temperature at the SWI was found to decrease considerably in the absence of HOx-induced mixing during periods when the HOx was turned off (Bryant *et al.*, 2011a). Conversely, it was shown that pH at the SWI was largely unaffected by HOx-induced changes in sediment O_2 concentrations (Bryant *et al.*, 2011b). It is therefore unlikely that pH was a major driver of community change in this system. pH remained between ~ 8 and 9 which, while relatively unfavorable for abiotic oxidation of Mn, is a favorable range for microbial oxidation (Crittenden *et al.*, 2005; Dellwig *et al.*, 2012). Oxygenation may also have affected food-web properties in the sediment, for example, by inducing changes in the population of bacterial grazers. Such indirect effects of HOx operation may have been insufficiently represented in the linear statistical model used for the ordination. Additionally, other factors limiting the explained variance may have been methodological, for example, that (1) sediment geochemical data may not have sufficiently represented microbial sediment samples because of localized

© 2011 Federation of European Microbiological Societies
Published by Blackwell Publishing Ltd. All rights reserved

sediment heterogeneity and/or (2) a large part of the observed variance was simply random or related to methodological noise. In future studies, a broader set of environmental variables, a higher-resolution evaluation of the microbial community structure (e.g. based on automated RISA or deep-sequencing approaches), and studies on the abundance of functional groups of microorganisms (e.g. by quantitative PCR targeting functional genes and their mRNA transcripts) might reveal additional information such as trends in less-abundant phylotypes and specific reactions of functional groups. However, these methods were outside of the scope of this study.

Presence of metal-oxidizers and reducers

Via PCR, sequencing/phylogenic analysis, and culturing on LBB medium, Fe- and Mn-reducing and Mn-oxidizing bacteria were confirmed to be members of the CCR sediment microbial community. The sample group evaluated for PCR-based detection of *Geobacteraceae* consisted of temporal end-points (12 July and 19 October) from the upper sediment (0–2 mm) and included all sites. Sequencing and phylogenetic analysis confirmed the presence of organisms with high sequence similarity to various *Geobacter* species, specifically *Geobacter chapellei* as well as *Pelobacter propionicus* which clusters with the genus *Geobacter* (Lonergan *et al.*, 1996; Fig. 7). Similar assemblages have previously been reported for freshwater sediment used as substrate in microbial fuel cells (Holmes *et al.*, 2004). The members of the genus *Geobacter*, including *Geobacter chapellei*, are well known metal-reducing bacteria. While the genus *Pelobacter* is mostly known for fermentative lifestyles, both *P. carbolicus* and *P. propionicus* have been shown to reduce Fe^{3+} (Lovley *et al.*, 1995; Lonergan *et al.*, 1996). *P. propionicus* has been found to have pili with a similar structure and close genetic relationship to the 'nanowire' conductive pili of *G. sulfurreducens* (Reguera *et al.*, 2005). PCR and sequencing/phylogenetic analyses thus confirmed the presence of a variety of metal-reducing organisms in CCR. Biological reduction of Mn in the anoxic sediment is expected to be a key process in the solubilization of the metal and thus for the upward flux of Mn into the water column (Thamdrup, 2000; Cummings *et al.*, 2003).

After confirming that *Geobacteraceae*, a well-characterized group of Fe- and Mn-reducers, were present in CCR, we were interested in whether the *Geobacteraceae* showed a dynamic response to HOx operation. Because of methodological difficulties, only a qualitative evaluation was possible. Real-time PCR indicated a decreased presence of *Geobacteraceae* in the upper sediment layer during the anoxic period as compared to the end of the oxygenation season, with the exception of site CCR-6 (Table 4). This is surprising, as *Geobacteraceae* are considered to be anaerobic. While recent genomic studies have indicated a capa-

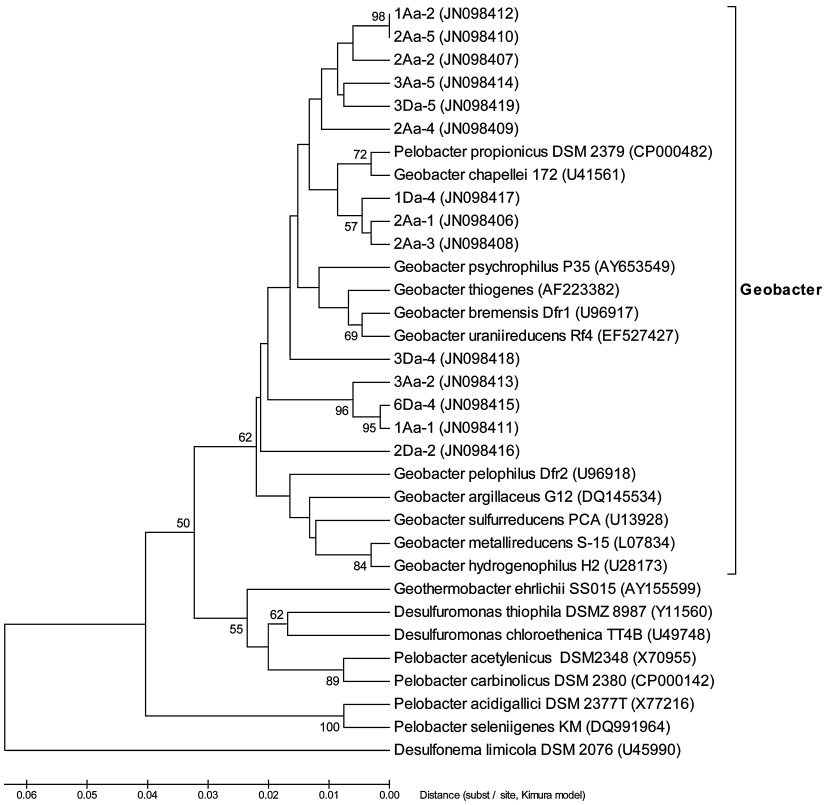

Fig. 7. Phylogenetic inference tree of clones obtained with *Geobacteraceae*-specific primers from CCR sediment and reference sequences. The tree was built using the UPGMA method. Branch labels indicate the percentage of 1000 bootstrap samplings supporting the branch topology of the shown consensus tree. The scale of branch length is in units of the number of base substitutions per site (subst/site) which are the same units as those of the evolutionary distances used to infer the phylogenetic tree (Kimura-2-parameter method; Tamura *et al.*, 2011). Clone names indicate the sample ID according to Table 1. All reference strains are type strains and are labeled with name and strain. Accession numbers are given in parentheses.

© 2011 Federation of European Microbiological Societies
Published by Blackwell Publishing Ltd. All rights reserved

Table 4. *Geobacteraceae* RTD-PCR results showing the presence of *Geobacteraceae* in the upper sediment layer (0–2 mm below the surface) after 1 month without oxygenation (12 July 2006) and 4 months with oxygenation (19 October 2006)

Site	Date	Sample ID	RTD-PCR
CCR-1	7/12/06	1Aa	–
CCR-2	7/12/06	2Aa	–
CCR-3	7/12/06	3Aa	–
CCR-6	7/12/06	6Aa	+
CCR-1	10/19/06	1Da	+
CCR-2	10/19/06	2Da	+
CCR-3	10/19/06	3Da	+
CCR-6	10/19/06	6Da	+

RTD-PCR results are scored '+' for presence and '–' for absence of amplifiable *Geobacteraceae* templates.

bility for aerobic metabolism (Methé *et al.*, 2003), several other factors may also have influenced our results. It is possible that the 1-month period of anoxia at the beginning of the study period was not long enough to support an increased community of anaerobic *Geobacteraceae* relative to the initial (pre-anoxia) community size. Additionally, the population size of *Geobacteraceae* may have been more strongly controlled by other factors (e.g. availability of sediment Fe- and Mn-oxides) than O_2 as also indicated for the microbial community as a whole by RDA results in Fig. 5. Enhanced precipitation of metal oxides as the oxygenation season progressed may have increased the availability of electron acceptors supporting *Geobacteraceae* growth. Furthermore, deposition and subsequent mineralization of fresh organic matter may have created anoxic 'hot spots' which could also have facilitated anaerobic communities in the upper sediment throughout the oxygenation season (Glud, 2008).

While Mn-oxidizers were not taxonomically identified or quantified, their presence and capacity for Mn-oxidation was confirmed via LBB analyses. Three of the 14 selected colonies were identified as Mn-oxidizers. The presence of Fe- and Mn-reducers as well as Mn-oxidizers confirms that Fe and Mn redox processes in CCR are influenced by metal-redox bacteria. Further investigation, however, is needed to more fully understand how oxygenation influences these bacteria specifically.

Conclusions

In summary, a pronounced response of the microbial community structure to oxygenation was only observed in near-surface sediment samples obtained near the HOx after 4 months of increasing oxygen-gas flow (Figs 5 and 6; Fig. S1). We found a significant correlation between these shifts in the sediment microbial community structure and environmental variables that changed in response to HOx operation (Figs 5 and 6). Additionally, nucleic acid concentrations in the sediment were typically elevated throughout the oxygenation season in regions most directly influenced by the HOx and at locations throughout the reservoir by the end of the campaign (Fig. 4). RTD-PCR indicated an increased presence of *Geobacteraceae* after oxygenation (Fig. 7). These data in combination with geochemical data showing increases in porewater concentrations of soluble Mn at the end of the oxygenation season (as precipitation of metal oxides increased) suggest enhanced activity and subsequent growth of the metal-reducing community (Figs 3 and 4; Table S3). Because a correlation between CCR HOx operation and the environmental variables themselves (e.g. porewater O_2 and soluble metal concentrations) has been observed in previous work (Bryant *et al.*, 2011a, b), the absence of an evident short-term shift in the microbial community structure in response to oxygenation may indicate that the considerable HOx-induced variation in sediment–water Fe and Mn dynamics (Fig. 3; Table S3; Bryant *et al.*, 2011b) was largely abiotically controlled (Stein *et al.*, 2002). Conversely, our results may be attributed to the ability of many bacteria to adapt to variations in sediment O_2 levels and utilize various electron acceptors, particularly over relatively short time scales (Thamdrup, 2000; Methé *et al.*, 2003). CCR had been continually oxygenated for the year prior to this campaign (Gantzer *et al.*, 2009a; Bryant *et al.*, 2011a). Hence, the microbial community may have been pre-adapted to oxic conditions. Longer-term oxygenation combined with a late-season influx of fresh organic matter may have been necessary to induce the changes observed in the microbial community on the final October sampling date.

Insight was obtained on the relative significance of the environmental and geochemical variables assessed in the CCR system. Of the variables evaluated, HOx flow, proximity to the HOx, sediment porewater O_2 and ferrous Fe concentrations, near-sediment soluble Fe concentrations, and total Mn levels in the bulk sediment were found to have the greatest influence on variation in community composition. Characterizing the effect of HOx operations on microbial and chemical processes controlling sediment–water fluxes of chemicals that impair water quality will ultimately (1) enhance understanding of environmental controls on sediment microbial community structure and (2) help optimize techniques used to manage lakes and reservoirs.

Acknowledgements

The authors are extremely grateful to Francisco Vasquez and Krista Köllner who offered invaluable advice and support with microbial techniques. We thank Francisco Vazquez for performing the cloning for *Geobacteraceae*

© 2011 Federation of European Microbiological Societies
Published by Blackwell Publishing Ltd. All rights reserved

sequence analysis. Biswarup Mukhopadhyay gave advice on sampling strategy and preservation. We thank Mary-Theresa Pendergast, Jose Manuel Cerato, Deric Learman, and Joseph Falkinham for assistance in isolation of Mn-oxidizing bacteria. Robert Rebodos assisted with ferrozine analyses. Paul Gantzer, Lindsay Olinde, Elizabeth Rumsey, and the staff at Western Virginia Water Authority provided help in the field and with laboratory samples. Alfred Wüest kindly reviewed the manuscript prior to submission. The manuscript was also greatly improved by feedback from two anonymous reviewers. The research described in this paper resulted from a shared contribution by the authors. This publication is based upon work supported by the National Science Foundation (NSF) under grants EAR-PF 0848123, DGE 504196, and CBET 1033514, the Western Virginia Water Authority, and Eawag.

References

Anderson RT, Rooney-Varga JN, Gaw CV & Lovley DR (1998) Anaerobic benzene oxidation in the Fe(III) reduction zone of petroleum-contaminated aquifers. *Environ Sci Technol* **32**: 1222–1229.

Angeler DG (2009) Species-specific and context-dependant disruption of temporal population fluctuations resulting from hypereutrophication events. *Environ Pollut* **157**: 3174–3182.

Balzer W (1982) On the distribution of iron and manganese at the sediment/water interface: thermodynamic versus kinetic control. *Geochim Cosmochim Acta* **46**: 1153–1161.

Beutel MW (2003) Hypolimnetic anoxia and sediment oxygen demand in California drinking water reservoirs. *Lake Reserv Manag* **19**: 208–221.

Beutel MW & Horne AJ (1999) A review of the effects of hypolimnetic oxygenation on lake and reservoir water quality. *J Lake Reserv Manag* **15**: 285–297.

Beutel MW, Hannoun I, Pasek J & Kavanagh KB (2007) Evaluation of hypolimnetic oxygen demand in a large eutrophic raw water reservoir, San Vincente Reservoir, Calif. *J Environ Eng-ASCE* **133**: 130–138.

Borcard D, Gillet F & Legendre P (2011) *Numerical Ecology with R*. Springer, New York.

Borneman J & Triplett EW (1997) Molecular microbial diversity in soils from eastern Amazonia: evidence for unusual microorganisms and microbial population shifts associated with deforestation. *Appl Environ Microbiol* **63**: 2647–2653.

Brendel PJ & Luther GW (1995) Development of gold mercury amalgam microelectrodes for the determination of dissolved Fe, Mn, O_2, and S(-II) in porewaters or marine and freshwater sediments. *Environ Sci Technol* **29**: 751–761.

Bryant LD, Lorrai C, McGinnis DF, Brand A, Wüest A & Little JC (2010) Variable sediment oxygen uptake in response to dynamic forcing. *Limnol Oceanogr* **55**: 950–964.

Bryant LD, Gantzer PA & Little JC (2011a) Increased sediment oxygen uptake caused by oxygenation-induced hypolimnetic mixing. *Water Res* **45**: 3692–3703.

Bryant LD, Hsu-Kim H, Gantzer PA & Little JC (2011b) Using source water as the solution: controlling Mn release at the sediment-water interface via hypolimnetic oxygenation. *Water Res* **46**: 6381–6392.

Buesing N, Filippini M, Bürgmann H & Gessner MO (2009) Microbial community structure in various habitats of a freshwater marsh. *FEMS Microbiol Ecol* **69**: 84–97.

Bürgmann H, Pesaro M, Widmer M & Zeyer J (2001) A strategy for optimizing quality and quantity of DNA extracted from soil. *J Microbiol Meth* **45**: 7–20.

Bürgmann H, Jenni S, Vazquez F & Udert KM (2011) Regime shifts and microbial dynamics in a sequencing batch reactor for nitrification and anammox treatment of urine. *Appl Environ Microbiol* **77**: 5897–5907.

Cerrato JM, Falkinham JO, Dietrich AM, Knocke WR, McKinney CW & Pruden A (2010) Manganese-oxidizing and -reducing microorganisms isolated from biofilms in chlorinated drinking water systems. *Water Res* **44**: 3935–3945.

Christian BW & Lind OT (2007) Multiple carbon substrate utilization by bacteria at the sediment-water interface: seasonal patterns in a stratified eutrophic reservoir. *Hydrobiologia* **586**: 43–56.

Clesceri LS, Greenberg AE & Eaton AD (1998) *Standard Methods for the Examination of Water and Wastewater*, 20th edn. American Public Health Association, Washington, DC.

Coppi MV, Leang C, Sandler SJ & Lovley DR (2001) Development of a genetic system for *Geobacter sulfurreducens*. *Appl Environ Microbiol* **67**: 3180–3187.

Crittenden JC, Trussell RR, Hand DW, Howe KJ & Tchobanoglous G (2005) *Water Treatment: Principles and Design*. John Wiley & Sons, New York.

Cummings DE, Snoeyenbos-West OL, Newby DT, Niggemyer AM & Lovely DR (2003) Diversity of *Geobacteraceae* species inhibiting metal-polluted freshwater lake sediments ascertained by 16S rRNA analysis. *Microb Ecol* **46**: 257–269.

Dalsgaard T, Nielsen LP, Brotas V *et al.* (2000) *Protocol Handbook for NICE – Nitrogen Cycling in Estuaries: A Project Under the EU Research Programme: Marine Science and Technology (MAST III)* (Dalsgaard T, ed), National Environmental Research Institute, Silkeborg, Denmark. http://www2.dmu.dk/LakeandEstuarineEcology/nice/NICE_handbook.pdf.

Davison W (1985) Conceptual models for transport at a redox boundary. *Chemical Processes in Lakes* (Stumm W, ed), pp. 31–53. John Wiley & Sons, New York.

Dellwig O, Schnetger B, Brumsack H-J, Grossart H-P & Umlauf L (2012) Dissolved reactive manganese at pelagic redoxclines (part II): hydrodynamic conditions for accumulation. *J Mar Syst* **90**: 31–41.

DiChristina TJ & DeLong EF (1993) Design and application of rRNA-targeted oligonucleotide probes for the dissimilatory iron- and manganese-reducing bacterium *Shewanella putrefaciens*. *Appl Environ Microbiol* **59**: 4152–4160.

© 2011 Federation of European Microbiological Societies
Published by Blackwell Publishing Ltd. All rights reserved

Environmental Protection Agency (EPA) (1988) *Determination of Total Organic Carbon in Sediment (Lloyd Khan Method). EPA Region II*. www.dnr.mo.gov/ENV/hwp/docs/part4sec5_lloydkahn_tocmethod.pdf.

EPA (1996) *Test methods for evaluating solid waste: physical/chemical methods, SW 846. Method 3050B: Acid digestion of sediments, sludges, and soils and Method 6010B: Inductively coupled plasma-atomic emission spectrometry, Rev. 2*. www.epa.gov/epaoswer/hazwaste/test/main.htm.

Falkowski PG, Fenchel T & Delong EF (2008) The microbial engines that drive earth's biogeochemical cycles. *Science* **320**: 1034–1038.

Fisher MM & Triplett EW (1999) Automated approach for ribosomal intergenic spacer analysis of microbial diversity and its application to freshwater bacterial communities. *Appl Environ Microbiol* **65**: 4630–4636.

Gantzer PA, Bryant LD & Little JC (2009a) Effect of hypolimnetic oxygenation on oxygen depletion rates in two water-supply reservoirs. *Water Res* **43**: 1700–1710.

Gantzer PA, Bryant LD & Little JC (2009b) Controlling soluble iron and manganese in a water-supply reservoir using hypolimnetic oxygenation. *Water Res* **43**: 1285–1294.

Glud RN (2008) Oxygen dynamics of marine sediments. *Mar Biol Res* **4**: 243–289.

Glud RN, Stahl H, Berg P, Wenzhöfer F, Oguri K & Kitazato H (2009) *In situ* microscale variation in distribution and consumption of O_2: a case study from a deep ocean margin sediment (Sagami Bay, Japan). *Limnol Oceanogr* **54**: 1–12.

Greenberg AE, Clesceri LS & Eaton AD (1992) Inductively coupled plasma-atomic emission spectrometry. *Standard Methods for the Examination of Water and Wastewater*, Method SM2540B, 18th edn. American Public Health Association, Washington, DC.

Hartmann M, Frey B, Kölliker R & Widmer F (2005) Semi-automated genetic analyses of soil microbial communities: comparison of T-RFLP and RISA based on descriptive and discriminative statistical approaches. *J Microbiol Meth* **61**: 349–360.

Hesslein R (1976) An in-situ sampler for close interval porewater studies. *Limnol Oceanogr* **21**: 912–914.

Holmes DE, Finneran KT, O'Neill RA & Lovley DR (2002) Enrichment of members of the family *Geobacteraceae* associated with stimulation of dissimilatory metal reduction in uranium-contaminated aquifer sediments. *Appl Environ Microbiol* **68**: 2300–2306.

Holmes DE, Bond DR, O'Neill RA, Reimers CE, Tender LM & Lovley DR (2004) Microbial communities associated with electrodes harvesting electricity from a variety of aquatic sediments. *Microb Ecol* **48**: 178–190.

House WA (2003) Factors influencing the extent and development of the oxic zone in sediments. *Biogeochemistry* **63**: 317–333.

Jørgensen BB & Boudreau BP (2001) Diagenesis and sediment-water exchange. *The Benthic Boundary Layer: Transport Processes and Biogeochemistry* (Boudreau BP & Jørgensen BB, eds), pp. 211–244. Oxford University Press, New York.

Kindt R & Coe R (2005) *Tree Diversity Analysis: A Manual and Software for Common Statistical Methods for Ecological and Biodiversity Studies*. World Agroforestry Centre (ICRAF), Nairobi.

Kohl PM & Medlar SJ (2006) *Occurrence of Manganese in Drinking Water and Manganese Control*. AWWA and USEPA. IWA Publishing, Philadelphia, PA.

Koizumi Y, Takii S & Fukui M (2004) Depth-related change in archaeal community structure in a freshwater lake sediment as determined with denaturing gradient gel electrophoresis of amplified 16S rRNA genes and reversely transcribed rRNA fragments. *FEMS Microbiol Ecol* **48**: 285–292.

Lewandowski J, Rüter K & Hupfer M (2002) Two-dimensional small-scale variability of pore water phosphate in freshwater lakes: results from a novel dialysis sampler. *Environ Sci Technol* **36**: 2039–2047.

Liboriussen L, Søndergaard M, Jeppesen E, Thorsgaard I, Grünfeld S, Jakobsen TS & Hansen K (2009) Effects of hypolimnetic oxygenation on water quality: results from five Danish lakes. *Hydrobiologia* **625**: 157–172.

Lonergan D, Jenter H, Coates J, Phillips E, Schmidt T & Lovley DR (1996) Phylogenetic analysis of dissimilatory Fe (III)-reducing bacteria. *J Bacteriol* **178**: 2402–2408.

Lorke A, Müller B, Maerki M & Wüest A (2003) Breathing sediments: the control of diffusive transport across the sediment-water interface by periodic boundary-layer turbulence. *Limnol Oceanogr* **48**: 2077–2085.

Lovley DR (1991) Dissimilatory Fe(III) and Mn(IV) reduction. *Microbiol Rev* **55**: 259–287.

Lovley DR, Phillips EJ, Lonergan DJ & Widman PK (1995) Fe (III) and S0 reduction by *Pelobacter carbinolicus*. *Appl Environ Microbiol* **61**: 2132–2138.

Mantel N (1967) The detection of disease clustering and a generalized regression approach. *Cancer Res* **27**: 209–220.

McGinnis DF & Little JC (2002) Predicting diffused-bubble oxygen transfer rate using the discrete-bubble model. *Water Res* **36**: 4627–4635.

McGinnis DF, Lorke A, Wüest A, Stöckli A & Little JC (2004) Interaction between a bubble plume and the near field in a stratified lake. *Water Resour Res* **40**: W10206, DOI: 10.1029/2004WR003038.

Methé BA, Nelson KE, Eisen JA *et al.* (2003) Genome of *Geobacter sulfurreducens*: metal reduction in subsurface environments. *Science* **302**: 1967–1969.

National Research Council (NRC) (2004) *Confronting the Nation's Water Problems: The Role of Research*. National Academies Press, Washington, DC.

Nealson KH (1997) Sediment bacteria: who's there, what are they doing, and what's new? *Annu Rev Earth Planet Sci* **25**: 403–434.

Nealson KH & Saffarini D (1994) Iron and manganese in anaerobic respiration: environmental significance, physiology, and regulation. *Annu Rev Microbiol* **48**: 311–343.

Nealson KH, Tebo BM & Rosson RA (1988) Occurrence and mechanisms of microbial oxidation of manganese. *Adv Appl Microbiol* **33**: 279–319.

© 2011 Federation of European Microbiological Societies
Published by Blackwell Publishing Ltd. All rights reserved

Nocker A, Burr M & Camper AK (2007) Genomic microbial community profiling: a critical technical review. *Microb Ecol* **54**: 276–289.

Oksanen J, Kindt R, Legendre P, O'Hara B, Simpson GL, Solymos P, Stevens MHH & Wagner H (2009) *VEGAN: community ecology package. R package version 1.15-3*. http://CRAN.R-project.org/package=vegan.

R Development Core Team (2009) *R: A Language and Environment for Statistical Computing*. R Foundation for Statistical Computing, Vienna, Austria. www.R-project.org.

Reguera G, McCarthy KD, Mehta T, Nicoll JS, Tuominen MT & Lovley DR (2005) Extracellular electron transfer via microbial nanowires. *Nature* **435**: 1098–1101.

Santschi P, Höhener P, Benoit G & Buchholtz-ten Brink M (1990) Chemical processes at the sediment-water interface. *Mar Chem* **30**: 269–315.

Schaller T & Wehrli B (1997) Geochemical-focusing of manganese in lake sediments – an indicator of deep-water oxygen conditions. *Aquat Geochem* **2**: 359–378.

Sigler WV, Crivii S & Zeyer J (2002) Bacterial succession in glacial forefield soils characterized by community structure, activity and opportunistic growth dynamics. *Microb Ecol* **44**: 306–316.

Singleton VL & Little JC (2006) Designing hypolimnetic aeration and oxygentation systems: a review. *Environ Sci Technol* **40**: 7512–7520.

Stein LY, La Duc MT, Grundl TJ & Nealson KH (2001) Bacterial and archaeal populations associated with freshwater ferromanganous micronodules and sediments. *Environ Microbiol* **3**: 10–18.

Stein LY, Jones G, Alexander B, Elmund K, Wright-Jones C & Nealson KH (2002) Intriguing microbial diversity associated with metal-rich particles from a freshwater reservoir. *FEMS Microbiol Ecol* **42**: 431–440.

Stookey LL (1970) Ferrozine – a new spectrophotometric reagent for iron. *Anal Chem* **42**: 779–781.

Tamura K, Peterson D, Peterson N, Stecher G, Nei M & Kumar S (2011) MEGA5: Molecular Evolutionary Genetics Analysis using maximum likelihood, evolutionary distance, and maximum parsimony methods. *Mol Biol Evol* **28**: 2731–2739.

Tebo BM & Emerson SR (1986) Microbial manganese(II) oxidation in the marine environment: a quantitative study. *Biogeochemistry* **2**: 149–161.

Tebo BM, Clement BG & Dick GJ (2007) Biotransformations of manganese. *Manual of Environmental Microbiology*, 3rd edn (Hurst C, Crawford R, Garland J, Lipson D, Mills A & Stetzenbach L, eds), pp. 1223–1238. ASM Press, Washington, DC.

Thamdrup B (2000) Bacterial manganese and iron reduction in aquatic sediments. *Advances in Microbial Ecology* (Schink B, ed), pp. 41–84. Kluwer Academic/Plenum Publishers, New York.

Van Cappellen P, Viollier E, Roychoudhury A, Clark L, Ingall E, Lowe K & DiChristina T (1998) Biogeochemical cycles of manganese and iron at the oxic-anoxic transition of a stratified marine basin (Orca Basin, Gulf of Mexico). *Environ Sci Technol* **32**: 2931–2939.

Viollier E, Inglett PW, Hunter K, Roychoudhury AN & Van Cappellen P (2000) The ferrozine method revisited: Fe(II)/Fe(III) determination in natural waters. *Appl Geochem* **15**: 785–790.

Widmer F, Rasche F, Harmann M & Fliessbach A (2006) Community structure and substrate utilization of bacteria in soils and conventional farming systems of the DOK long term field experiment. *Appl Soil Ecol* **33**: 294–307.

Wüest A, Brooks NH & Imboden DM (1992) Bubble plume modeling for lake restoration. *Water Resour Res* **28**: 3235–3250.

Yannarell AC & Triplett EW (2005) Geographic and environmental sources of variation in lake bacterial community composition. *Appl Environ Microbiol* **71**: 227–239.

Yannarell AC, Kent AD, Lauster GH, Kratz TK & Triplett EW (2003) Temporal patterns in bacterial communities in three temperate lakes of different trophic status. *Microb Ecol* **46**: 391–405.

Zaw M & Chiswell B (1999) Iron and manganese dynamics in lake water. *Water Res* **33**: 1900–1910.

Zhang H, Davison W & Ottley C (1999) Remobilisation of major ions in freshly deposited lacustrine sediment at overturn. *Aquat Sci* **61**: 354–361.

Supporting Information

Additional Supporting Information may be found in the online version of this article:

Fig. S1. Average linkage hierarchical cluster analysis of community similarity (Bray dissimilarity) of CCR sediment samples based on normalized bandintensity data of RISA phylotypes.

Table S1. Variability as characterized by standard deviation (σ) and replicate measurements (m) for average CCR-1 O_2 concentration data presented in Fig. 2.

Table S2. Variability as characterized by standard deviation (σ), replicate measurements (m), and error in measurement for average CCR-1 O_2, Fe, Mn, and TOC data presented in Fig. 3.

Table S3. Chemistry data for sediment and overlying water throughout 2006 oxygenation season in CCR.

Please note: Wiley-Blackwell is not responsible for the content or functionality of any supporting materials supplied by the authors. Any queries (other than missing material) should be directed to the corresponding author for the article.

© 2011 Federation of European Microbiological Societies
Published by Blackwell Publishing Ltd. All rights reserved